# In-Band Full-Duplex Free-Space Optical Transceiver Design for Flying Platforms

Md Sarwar Uddin Chowdhury and Murat Yuksel Electrical and Computer Engineering, University of Central Florida, Orlando, FL mdsarwaruddin.chowdhury@ucf.edu, murat.yuksel@ucf.edu

Abstract-Free-space optical (FSO) communication is one of the crucial branches of wireless communication that utilizes light to transmit signals through the air. Being an essential element of the FSO system, the transceiver design plays a vital role in sending and receiving optical signals. In this work, we propose a multi-element transceiver design that can be a potential solution for improving FSO communication link effectiveness for mobile platforms such as Unmanned Aerial Vehicles (UAVs). We formulate the problem of placing optoelectronic transmitters (e.g., lasers or Light Emitting Diodes (LEDs)) and receivers (e.g., photodetectors (PDs)) on a transceiver plane. The formulation aims to maximize the Signal-to-Interference-plus-Noise Ratio (SINR) among two hovering UAVs. Applying the Genetic Algorithm (GA) for optimization, we show that the SINR is maximized when 43% of the transceiver plane is covered with lasers with 5 mRad divergence. We show that, at certain link ranges, a particular pattern of laser placement on the transceiver plane gives result to the best performance, making it possible to replicate the transceiver design for multiple platforms without having to perform mechanical steering.

Index Terms—Free-space optical, In-band Full-duplex, Laser, Multi-element, Transceiver, UAV

#### I. Introduction

Over the last few decades, Unmanned Aerial Vehicles (UAVs) have come into the limelight in wireless communication due to their mobility and flexibility. They have the potential to supplement traditional fixed networks and open new opportunities in various communication applications. For instance, when traditional communication systems become out of order or damaged during natural disasters or emergencies, UAV-mounted infrastructure can be helpful as a backup communication system. Also, UAVs have the potential to be used in disaster zones for faster communication between rescue teams and volunteers [1].

UAVs communicating via legacy radio frequency (RF) have a maximum data transfer rate of about 274 Mbps [2]. The increased demand for bandwidth and capacity requirements for UAV-to-UAV communication inspired the concept of using FSO communication (FSOC). Besides the enlarged capacity, FSOC connectivity is very secure and requires an appropriately aligned matching transceiver to complete the transmission. The narrow and invisible optical beams make them immune to detection and interception. Despite these unique benefits, FSOC faces challenges, like vulnerability to adverse weather conditions (e.g., smoke, fog, dust, and rain) and requiring

This work has been supported in part by United States National Science Foundation award 2115215.

a direct line-of-sight between transmitter (TX) and receiver (RX). The optical wave can be attenuated by absorption, scattering, and turbulence. It needs precise alignment and can be affected by factors such as misalignment due to environmental factors or vibrations. Designing a multi-element transceiver with tolerance for mobility, sway, vibration, or tilt during communication and beam steering, spatial reuse, and adaptive optimization capabilities can be helpful to some extent in overcoming these challenges.

The advantages FSOC offers can be utilized more effectively by in-band full-duplex (IBFD) communication than out-of-band communication. IBFD attains more efficient spectrum utilization, reduced latency, improved system capacity, and overall throughput. However, there are challenges associated with IBFD FSOC too. Managing the impact of simultaneous transmission and reception within the same frequency band needs to be addressed. This typically boils down to self-interference (SI) cancellation. Hence, an IBFD multi-element FSOC transceiver design must consider the SI imposed by the placement of TXs and optimize the design accordingly.

# A. Contributions

In this work, we present an IBFD multi-element FSO transceiver design for flying platforms such as quadcopters or high-altitude platforms. We envision a replicate of the transceiver to be mounted on each flying platform. The aim is to maximize the SINR of the link between two such IBFD FSO transceivers. We consider a square-shaped transceiver plane covered with transmitters (lasers) or receivers (photodetectors). We formulate the SINR maximization problem in terms of the number of transmitter elements and their positions on the transceiver plane. We design a Genetic Algorithm (GA) to solve the problem while considering the vibration of the flying platforms where the transceivers are mounted. Using GA, we find the optimal transceiver design as divergence angle of the TX (and the field-of-view of the RX) elements or the distance between the transceivers vary. We show that after 40 m distance, a common optimum tiling pattern exists as the distance or divergence angle changes. This is a promising result as it means it will be possible to produce FSO transceivers with a common pattern and mount them on flying platforms without worrying about optimizing them for each platform. This approach eliminates the need for sensitive mechanical steering and tracking instruments to maintain the link between mobile platforms, which has

been the traditional approach in FSOC. Our work shows that, for flying or portable platforms, using a multi-element FSOC transceiver with an optimized placement of TX and RX elements is a more practical approach than a single-element design with mechanical tracking apparatus.

#### II. RELATED WORK

Full-duplex FSO transceivers, both in-band and out-ofband, have been reported in prior works. Recent interest has been drawn to IBFD FSOC designs because of their benefit over out-of-band designs. Although SI losses impact IBFD communication, proper design execution, and SI mitigating methods may boost channel capacity. Even with SI, fullduplex communication can offer at least a 20% improvement over half-duplex communication [3]. A full-duplex system that used VCSEL as the uplink transmission light source has been proposed by Wang et al. for indoor communication, where the transceiver deployed distinct wavelengths for uplink and downlink channels to suppress the SI [4]. Oh et al. reported an IBFD design, where communication between a stationary controller and a mobile node is established utilizing data erasure and beam reversibility technique [5]. The controller, however, has a TX and no RX, although the model performs full-duplex operation for mobile node.

In [3], [6], it is shown how an IBFD FSO transceiver can isolate an infrared TX and RX for drone communication where LEDs are used for transmission. A Multi-element IBFD transceiver using optimum tiling is reported by Haq et al. where lasers with much narrower beam widths and divergence angles are used for transmission [7]. In that work, the authors used two schemes. At first, they used an equidistant scheme where all TXs are placed equidistant from the center of the transceiver plane, and then considered the effects of variation of divergence angle, pointing error angle and vibration of UAV platform as in the form of vibration angle to determine the optimum number of TXs that could be placed on the transceiver plane. After that, they incorporated all the findings from that scheme into random positions scheme where TXs are placed randomly on the transceiver plane, and the optimization of TX positions was done by this scheme. Due to the intricate and heavy computational process of the random position scheme, at the end of the paper, the authors proposed GA based optimization technique which is applied for optimizing the positions of the TXs only. So, they imposed some constraints, like placing TXs equidistant from the transceiver plane while determining the optimized TXs number. In this work, we randomize the whole process without applying any such constraints and focus on optimizing both TX numbers as well as TX positions on the transceiver using GA.

# III. SYSTEM MODEL

For the evaluation and optimization of communication systems in diverse wireless applications, SINR offers a quantitative measure of the signal quality in relation to interference and noise. It is the key parameter for assessing the performance of a transceiver. Fig. 1 shows a simplified system model

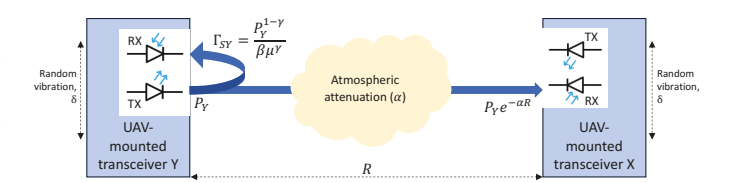


Fig. 1. Simplified system model: One IBFD transceiver on each side.

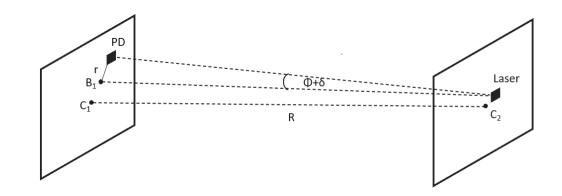


Fig. 2. Orientation of two transceiver planes after alignment.

consisting of two transceiver planes with a TX and an RX at each plane. Assume, two square-shaped transceivers X and Y, each having TXs with divergence angle  $\theta$  and RXs with detection area D, set up an FSOC link at distance R. To calculate the IBFD FSOC link's SINR, we need to consider the SI at each unit (e.g.,  $\Gamma_{SY}$  for transceiver Y) as shown in Fig. 1. Further, we need to consider the coupling efficiency, i.e., the amount of power received at the RXs.

If total transmit power at transceiver Y is denoted by  $P_Y$  then SINR for transceiver X can be expressed as [8]:

$$SINR_{Y\to X} = \left[ \frac{P_Y L_Z(R,\lambda) D \cos(\phi + \delta)}{(\tan \theta)^2 4R^2 (P_N + \Gamma_{SX})} \right]^2 \tag{1}$$

where  $L_Z(R,\lambda)$  is the free space loss parameter for a link range of R,  $\Gamma_{SX}$  is the residual SI power at transceiver X,  $P_N$  is the Noise Equivalent Power (NEP),  $\phi$  is the pointing error angle,  $\delta$  is the additional pointing error angle that arises from the vibration of the mobile platform. As detailed in [9],  $\alpha$  is a function of atmospheric visibility which we assumed 1km. As detailed in [7],  $P_N$  is a function of solar background shot noise, signal shot noise, and dark current shot noise. Following the same conventional noise values for low-flying drone operation and opto-electronic circuitry, we assumed  $P_N$  to be 0.29mW. We assume that the aperture area of an RX element is  $D=1 \text{cm}^2$ . By utilizing the residual SI model of [10] and [11], the SI power for transceivers X and Y can be written as  $\Gamma_{SX}=\frac{P_X^{(1-\gamma)}}{\beta\mu^\gamma}$  and  $\Gamma_{SY}=\frac{P_Y^{(1-\gamma)}}{\beta\mu^\gamma}$ , respectively. Here,  $\beta$  denotes the coefficient of SI suppression between TX and RX inside the same transceiver plane.  $\mu$  and  $\gamma$  are SI suppression parameters for passive SI cancellation approach.

When there are multiple TX and RX elements on the transceiver planes, the SINR calculation must consider the respective positions of the TX and RX elements. Due to the positions, the TX and RX elements have pointing error. As shown in Fig. 2, for a given TX on the transmit side, an RX on the receive side may not perfectly correspond to it and may be off by a pointing angle  $\phi$ . Further, due to vibration, there can be an additional pointing error, which we denote with  $\delta$ . For

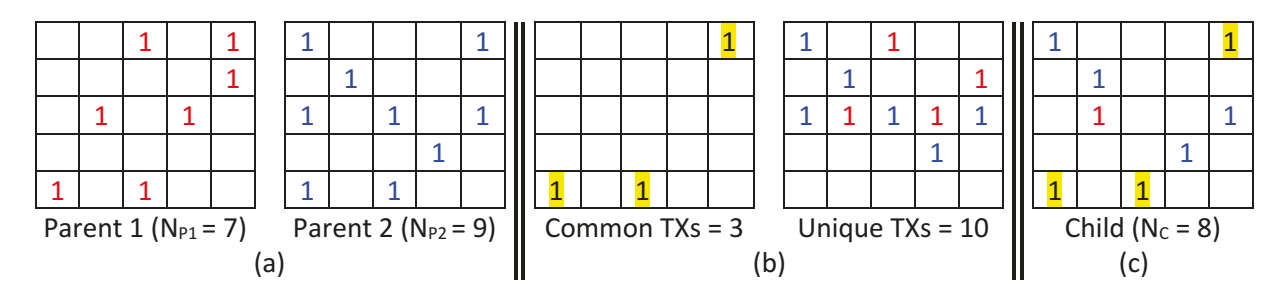


Fig. 3. An example illustrating GA's crossover steps: (a) Randomly selected two parents from fit population, (b) Common TXs and unique TXs Positions, (c) Child with all common TXs positions and rest of the TXs selected randomly from the unique positions.

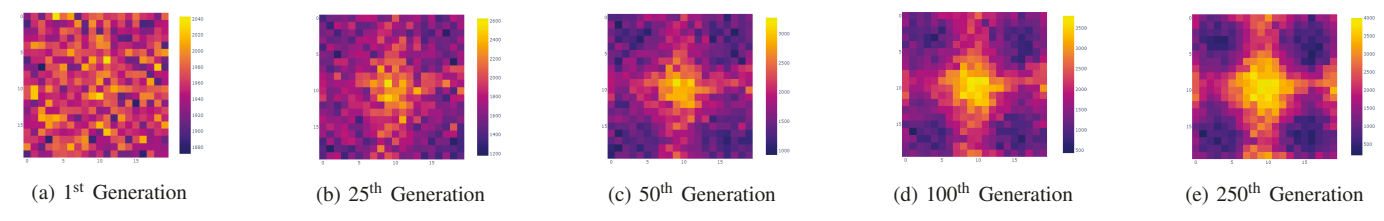


Fig. 4. Heatmaps of TX placements on a 20×20 transceiver grid for various generations of GA.

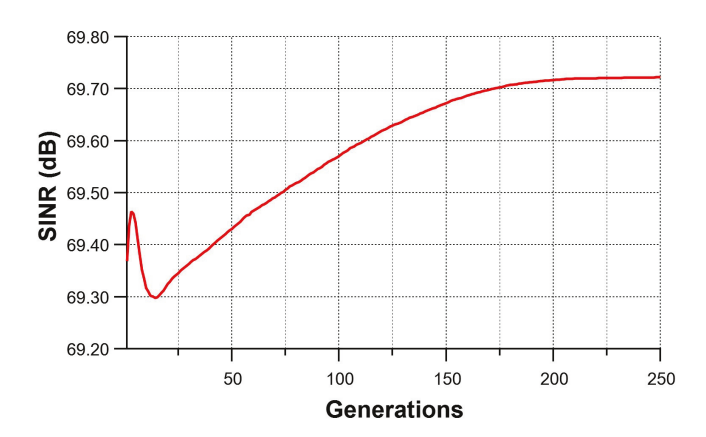


Fig. 5. SINR variation over 250 generations when R=50 m,  $\theta=5$  mrad,  $\delta=(0$  rad, 1 rad), and  $P_Y=1$  W (i.e.,  $\approx 6$  mW per transmitter).

multi-element FSO transceivers having N TXs and  $N_m-N$  RXs, we revise (1) to calculate the SINR while considering the aggregate received power as well as the aggregate noise. Assuming that the total transmit power is fixed at  $P_Y$ , the SI power (which is the noise in (1)) stays the same in the multi-element case. Likewise, the aggregate NEP  $P_N$  stays the same as well. Hence, the SINR for the multi-element FSOC link can be written as:

$$\overline{SINR} = \sum_{i=1}^{N} \sum_{j=1}^{N_m - N} SINR_{TX(i) \to RX(j)}$$
 (2)

where TX() and RX() are the sets of transmitters and receivers on the transceiver plane. When calculating  $SINR_{TX(i)\to RX(j)}$  above, we assume that each TX emits  $P_Y/N$  power and has the same divergence angle  $\theta$ .

Since we are considering a replica of the transceiver on each side, placing a TX on a position on the transceiver plane occupies the reception aperture for that position. Hence, maximizing SINR in (2) involves tuning the number N as well as placement of TXs on the transceiver plane. Let  $\mathcal{P}_{1\times N}$  be the list of positions of the TXs on the transceiver plane. Then, we can write the SINR maximization problem for an IBFD transceiver with  $N_m$  TX or RX elements on it as follows:

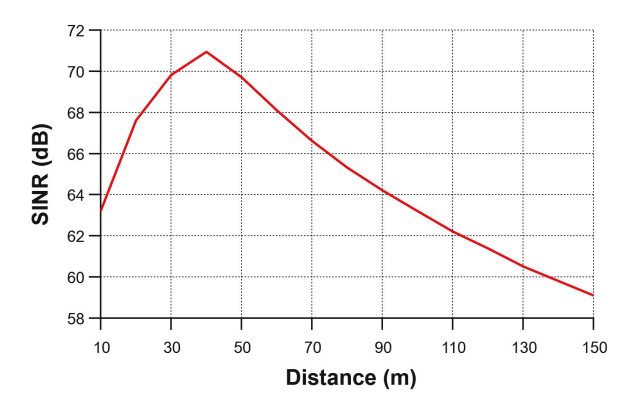
$$\max_{N,\mathcal{P}} \overline{SINR} \tag{3}$$

such that 
$$0 < N < N_m$$
. (4)

The constraints (4) of the SINR maximization problem above make sure that there is at least one TX on the plane. The search space for this problem is quite large, i.e.,  $2^{N_m}-2$ . Since each possible solution requires  $NN_m$  computations per (2), the overall complexity is  $\mathcal{O}(N_m^2 2^{N_m})$ . Further, this computational complexity does not consider the random vibration effect, which requires Monte Carlo simulations to quantify the SINR in (1). Hence, we resort to global optimization methods to get a solution to the problem.

# IV. GENETIC ALGORITHM (GA) DESIGN

We used GA for determining the number of TXs and TX positions on the transceiver plane. We apply this algorithm because it helps us reach the optimum solution faster by reducing the computational complexity and is also good at exploring the entire search space to find the global optimum. To implement GA, we first initialize the transceiver plane, which is divided into a  $20\times20$  grid that offers 400 positions for placing TXs or RXs. We randomly generate a population with 500 solutions (i.e. individuals) in it. Each solution has a randomly generated TX count between 1 and 399, which guarantees that each solution has at least one TX to transmit



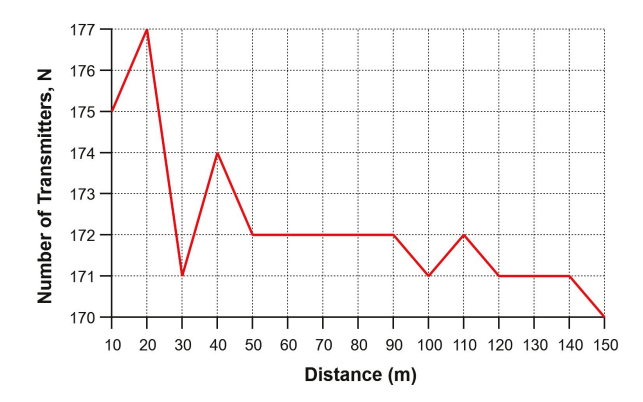


Fig. 6. SINR vs. distance when  $\theta$  = 5 mrad,  $\delta$  = (0 rad, 1 rad),  $P_Y$  = 1 W (i.e.,  $\approx$ 6 mW per transmitter), (b) Optimized TX count for different R, when  $\theta$  = 5 mrad,  $\delta$  = (0 rad, 1 rad),  $P_Y$  = 1 W (i.e.,  $\approx$  6 mW per transmitter)

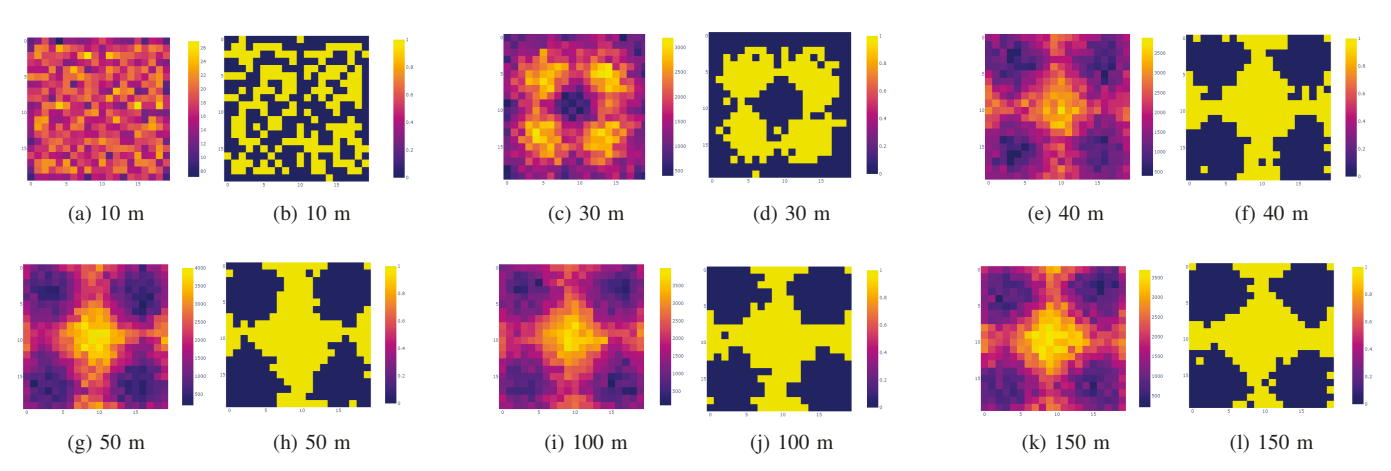


Fig. 7. Heatmaps and corresponding optimized transceiver planes for various distances.

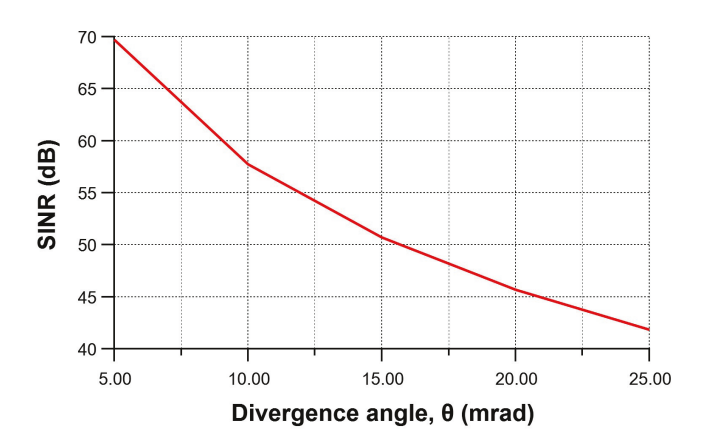


Fig. 8. SINR vs. divergence angle  $\theta$  when R = 50 m,  $\delta$  = (0 rad, 1 rad) ,  $P_Y$  = 1 W (i.e.,  $\approx$  6 mW per transmitter)

the signal and at least one RX to receive the signal. After that, we determine SINR for each solution based on (2). Then, to select the fit population, we pick the top 20% of the solutions attaining the highest SINR values.

Crossover: Given a fit population, we apply a crossover

method to construct the next generation with 500 members in it. To create a member of the next generation, we randomly choose two individuals from the existing fit population and apply the following steps to perform the crossover: Let the number of TXs of the two randomly picked parents be  $N_{P1}$  and  $N_{P2}$ . We calculate the number of TXs for the child by taking the floor of the average of the two parents, i.e.,  $N_C = \lfloor (N_{P1} + N_{P2})/2 \rfloor$ . Then, we find the common TX positions of the two parents and keep those positions in the child. To complete the TX count for the child to  $N_C$ , we randomly pick the rest of the TX positions from the unique position of TXs available in two parents. Fig. 3 shows the crossover steps for a  $5\times 5$  transceiver size. This process is repeated to compose the entirety of the next generation.

Stopping Criterion: In our simulations, we observed that 250 generations was sufficient to converge the evolution. Fig. 5 shows the average SINR of the fit population as GA progresses over generations. As expected, the GA first explores the search space, which cause some reduction in the average SINR; but later it converges due to the selection of common TX positions in the crossovers. It is evident that 250 generations is sufficient to attain a converged population.

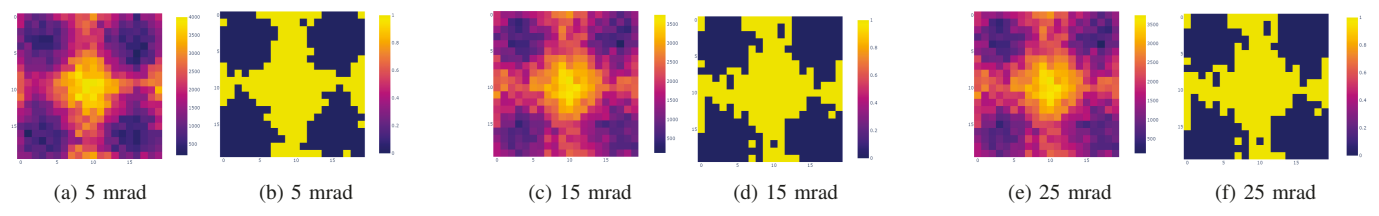


Fig. 9. Heatmaps and corresponding optimized transceiver planes for different divergence angles,  $\theta$ .

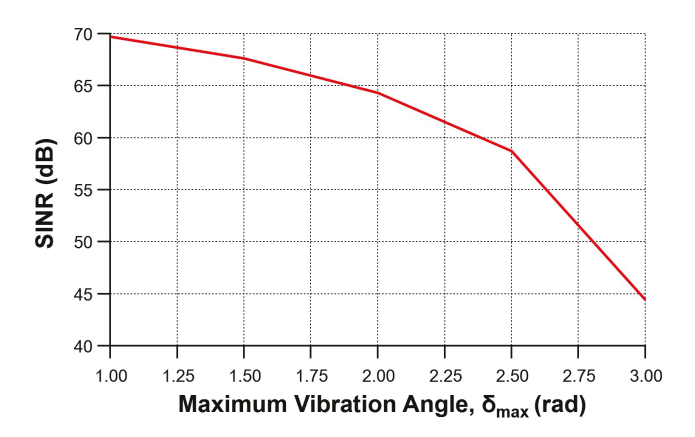


Fig. 10. SINR vs. maximum vibration error  $\delta_{max}$  when R = 50 m,  $\theta$  = 5 mrad,  $P_Y$  = 1 W (i.e.,  $\approx$ 6 mW per transmitter).

Picking the Best Solution: To eliminate the random selections of the GA, we ran it 40 times. However, this raises the issue of selecting the best solution among these runs. To address this issue, we generated a heatmap of the TX positions for each solution in the fit populations from each GA run. Fig. 4 shows how this heatmap evolves over GA generations. Given a heatmap of TX positions, we, then, calculate (the floor of) the average TX count among all solutions in the fit populations of 40 GA runs. For example, when R = 50 m, this average turned out to be 172 positions (43%) after 250 generations. Based on this, to construct the best transceiver design, we pick the most popular 172 TX locations from the heatmap. Fig. 7 shows the heatmaps and the corresponding best transceiver design for various R. From Fig. 4, we observe that with the progress of the generations, the TXs start to accumulate to form a plusshaped pattern, with more TXs concentrated at the center and four ends of the four arms of the shape. The intuition of such shapes is that the central transmitters can provide coverage to a large portion of the square shaped transceiver plane, while the transmitters of the four arms with relatively high concentration at the four ends help to fill in the coverage gaps. It is seen that some transmitters are placed around the edges. Center of the beams of those transmitters might fall outside the plane under the presence of vibration and energy from such beam might not be fully detected. Yet such placement is important to ensure that the transceiver receives a significant signal quality.

#### V. RESULTS AND EVALUATION

In our multi-element transceiver design, we aim to optimize SINR by tuning the number of TXs and their positions in transceiver plane. To study the IBFD communication between two UAVs, we create a simulation environment in Python where we can vary some of the critical parameters including the link distance (i.e., the distance between the two UAVs), the divergence angle (or field-of-view) of the TXs and RXs. and the vibration amounts of the UAVs. The wavelength is set to 900 nm. The square-shaped transceiver plane is divided into 20  $\times$  20 grid, forming a 20 cm  $\times$  20 cm plane with each TX or RX element occupying  $D = 1 \text{ cm}^2$ . To reduce the computational complexity and simulation time, we used GA for optimization as detailed in the previous section. As GA is working over its generations, we will discuss the changes in SINR and the best observed TX positions while varying the link distance (R), the divergence angle ( $\theta$ ) of TXs (which is also the field-of-view of the RXs), and the maximum vibration angle  $(\delta)$  of the UAVs.

#### A. Effect of Link Distance, R

Depending on the current distance between the transceivers, the best attainable SINR may or may not increase when the UAVs move closer to each other. Fig. 6(a) shows this result by plotting the effect of varying R on average SINR. The figure shows the best attainable SINR after transceiver design is optimized by the GA. When R < 40m, increasing the distance between the UAVs increases the best average SINR. However, for R larger than 40 m, reducing the distance between UAVs is needed to increase SINR. This outcome shows the trade-off between coupling efficiency of the transceiver design and the potential increase in the aggregate receivable signal strength.

Consider a particular TX i, which emits a Gaussian beam that creates a footprint on the receiver plane centered at the corresponding location of TX i and has a diameter of  $R \tan \theta$ . So, for 40 m range the beam footprint diameter is equal to the size of the grid and for this distance we see from Fig. 6(a) that SINR is maximum. After 40 m, with the increase of link distance average SINR drops almost exponentially. This is expected as the signal will be more attenuated due to absorption and scattering. On the other hand, the SINR is also decreased for the distance below 40 m. This is due to the fact that the diameter of the beam footprint becomes narrower as distance is reduced, a smaller beam footprint means that the energy of the transmitted signal is concentrated into a narrower area on the receiver plane. This can result in a reduction in the received signal power at the receiver. So, due to smaller coupling efficiency, SINR is decreased.

We find no significant change in number of TXs as R varies and, in every case, it is seen that the maximum SINR is

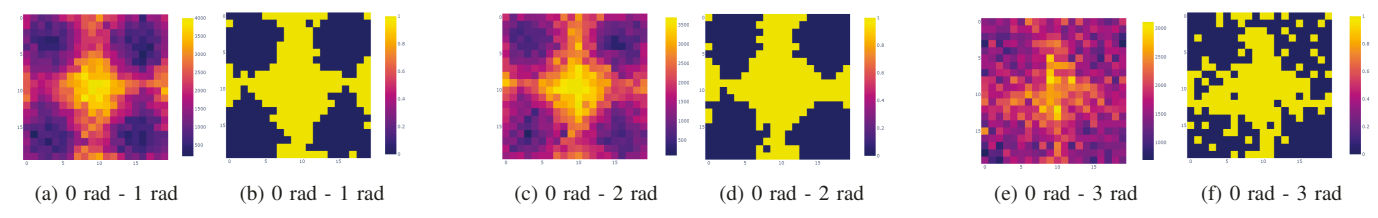


Fig. 11. Heatmaps and corresponding optimized transceiver planes for different vibration angles,  $\delta$ .

obtained when the TX count is almost 43% as shown in Fig. 6(b). The heatmap for each 10 m distance variation obtained from the simulation and, for simplicity, we only depicted some of them in Fig. 7. The fig. shows that, for 10 m to 40 m range, we have different patterns of TX placement. But, starting from 40 m the pattern becomes almost the same. If the distance is decreased below 40 m the beam footprint diameter is also decreased. As a result, we observe different patterns for different R. After 40 m, however, the receiver area under each beam footprint becomes almost same, so despite the increase of R, the pattern remains almost the same – indeed, we have seen only some minor adjustment of TX positions in the transceiver plane for the variation of R.

# B. Effect of Divergence Angle, $\theta$

One of the major benefits of FSOC systems is the ability to transmit a very narrow optical beam as it is possible to design TX devices with very low divergence angles. In our design we are assuming that the field-of-view of the RX elements is the same as the divergence angle of the TX elements, and hence, we vary them both at the same time. The impact of changing the divergence angle,  $\theta$ , for the elements is shown in Fig. 8 when the distance between the UAVs is 50 m. We observe an exponential reduction of SINR with the increase of  $\theta$ . Since, for this link distance, the entire footprint of the TX beams are falling on the receiver plane, the increase in  $\theta$  causes more diffraction means the beams spread out more and the RXs are only able to collect a smaller fraction of the beams. An interesting observation is that, even with the change of  $\theta$ , the link performance is optimum when the TX count remains 43% of the possible elements on the transceiver, and the TX positions on the transceiver plane remain almost unchanged as shown in Fig. 9.

# C. Effect of Vibration Angle, $\delta$

When the vibration angle,  $\delta$ , of the UAVs varies, the SINR-maximizing positioning of TXs in the transceiver plane also changes. To simulate the vibrations on the hovering UAVs, we randomly pick  $\delta$  between 0 and  $\delta_{max}$ . To observe the effect of  $\delta$  on the transceiver design we, then, vary  $\delta_{max}$ , the maximum vibration error. Fig. 10 depicts the impact of the vibration angle on the best attainable SINR when  $\delta_{max}$  varies from 1 to 3 rad. From the heatmaps shown in Fig. 11, we observe that as the vibration angle increases the positions of TXs become more scattered. The vibration causes misalignment which can lead to a degradation of Gaussian beam profile as the optimal alignment needed for the expected beam shape and focusing

may be compromised. As a result of beam misalignment, the coupling efficiency is decreased which affects the SINR performance. To compensate, the TX placement becomes more scattered on the transceiver plane.

# VI. CONCLUSION

A multi-element transceiver with a unique tiling pattern is proposed to establish UAV-UAV communication. SI, vibration of the mobile platform, are incorporated into the system model. A simulation environment in Python is created to simulate the model to achieve maximum SINR by optimizing TX counts and positions. By applying GA, we found that, for a  $20\times20$  grid, the best performance can be obtained if 43% of the transceiver plane is covered with TXs. Here, we saw the tiling of TXs form a plus-shaped pattern with a relatively high concentration of TXs at the center and at the ends of the four arms of the shape. The proposed multi-element transceiver could be useful in establishing UAV-UAV communication and help to develop portable FSOC without mechanical steering.

#### REFERENCES

- J.-H. Lee, K.-H. Park, Y.-C. Ko, and M.-S. Alouini, "A UAV-mounted free space optical communication: Trajectory optimization for flight time," *IEEE Transactions on Wireless Communications*, vol. 19, no. 3, pp. 1610–1621, 2019.
- [2] M. Khan and M. Yuksel, "Autonomous alignment of free-space-optical links between UAVs," in *Proc. of ACM HotWireless*, pp. 36–40, 2015.
- [3] A. S. Haq, M. R. Khan, and M. Yuksel, "A prototype of in-band full-duplex free-space optical transceiver," in *Proceedings of IEEE LANMAN*, pp. 112–113, 2018.
- [4] K. Wang, A. Nirmalathas, C. Lim, K. Alameh, and E. Skafidas, "Full-duplex gigabit indoor optical wireless communication system with CAP modulation," *IEEE Photonics Technology Letters*, vol. 28, no. 7, pp. 790–793, 2016.
- [5] C. W. J. Oh, Z. Cao, E. Tangdiongga, and T. Koonen, "10 Gbps all-optical full-duplex indoor optical wireless communication with wavelength reuse," in *Proceedings of OFC*, pp. 1–3, 2016.
- [6] A. S. Haq, M. Khan, and M. Yuksel, "Asynchronous los discovery algorithm for aerial nodes using in-band full-duplex transceivers," in *Proceedings of ACM CoNEXT*, pp. 26–28, 2019.
- [7] A. S. Haq and M. Yuksel, "Multi-element full-duplex fso transceiver design using optimum tiling," *Optics Comm.*, vol. 501, p. 127377, 2021.
- [8] J. W. Giles and I. N. Bankman, "Underwater optical communications systems. part 2: Basic design considerations," in *Proceedings of IEEE MILCOM*, pp. 1700–1705, 2005.
- [9] I. I. Kim, B. McArthur, and E. J. Korevaar, "Comparison of laser beam propagation at 785 nm and 1550 nm in fog and haze for optical wireless communications," in *Proceedings of SPIE, Optical wireless* communications III, vol. 4214, pp. 26–37, 2001.
- [10] M. Duarte, C. Dick, and A. Sabharwal, "Experiment-driven characterization of full-duplex wireless systems," *IEEE Transactions on Wireless Communications*, vol. 11, no. 12, pp. 4296–4307, 2012.
- [11] A. F. Haq and M. Yuksel, "Weather-limited in-band full-duplex transceiver model for free-space optical communication," *Optical Engineering*, vol. 59, no. 5, pp. 056113–056113, 2020.